CEAS Aeronautical Journal (2020) 11:501–513
https://doi.org/10.1007/s13272-019-00431-z

ORIGINAL PAPER

# Initial investigation into the complementary use of black box and physics-based techniques in rotorcraft system identification

**Susanne Seher-Weiß**[1] · **Johannes Wartmann**[1]

Received: 18 December 2018 / Revised: 27 September 2019 / Accepted: 25 October 2019 / Published online: 11 November 2019


**Abstract**
Accurate linear helicopter models are needed for control system development and simulation and can be determined by system identification when appropriate test data are available. Standard methods for rotorcraft system identification are the frequency domain maximum likelihood method and the frequency response method that are used to derive physics-based linear state-space models. Also the optimized predictor-based subspace identification method (PBSIDopt), a time domain system identification method that yields linear black box state-space models, has been successfully applied to rotorcraft data. As both methods have their respective strengths and weaknesses, it was tried to combine both techniques. The paper demonstrates the successful complementary use of physics-based frequency domain methods and the black box PBSIDopt method in the areas of database requirements, accuracy metrics, and model structure development using flight test data of DLR's ACT/FHS research rotorcraft.

**Keywords** System identification · Black box · Maximum likelihood · Predictor-based subspace

**List of symbols**

| | |
|---|---|
| $a_x$, $a_y$, $a_z$ | Longitudinal, lateral, and vertical acceleration (m/s$^2$) |
| $\boldsymbol{A}$, $\boldsymbol{B}$, $\boldsymbol{C}$, $\boldsymbol{D}$ | State-space matrices (continuous time) |
| $\mathrm{CR}_j$ | Cramer–Rao bound of the $j$th parameter |
| $\boldsymbol{\mathcal{F}}$ | Fischer information matrix |
| $J$ | Cost function |
| $L$, $M$, $N$ | Moment derivatives |
| $n$ | Model order |
| $n_y$ | Number of model outputs |
| $p$, $q$, $r$ | Roll, pitch and yaw rates (rad/s) |
| $\boldsymbol{R}$ | Measurement noise covariance matrix |
| $u$, $v$, $w$ | Airspeed components (aircraft fixed) (m/s) |
| $\boldsymbol{u}$, $\boldsymbol{x}$, $\boldsymbol{y}$ | Input, state, and output vectors |
| $X$, $Y$, $Z$ | Force derivatives |
| $\delta_{\mathrm{lon}}$, $\delta_{\mathrm{lat}}$ | Longitudinal and lateral cyclic inputs (%) |
| $\delta_{col}$, $\delta_{\mathrm{ped}}$ | Collective and pedal inputs (%) |
| $\phi$, $\theta$ | Roll and pitch attitude angles (rad) |
| $\boldsymbol{\Theta}$ | Unknown model parameters |

**Abbreviations**

| | |
|---|---|
| ACT/FHS | Active control technology/flying helicopter simulator |
| CR | Cramer–Rao |
| DLR | German Aerospace Center |
| FR | Frequency response |
| ML | Maximum likelihood |
| PBSIDopt | Optimized predictor-based subspace identification (method) |

✉ Susanne Seher-Weiß
susanne.seher-weiss@dlr.de

Johannes Wartmann
johannes.wartmann@dlr.de

[1] German Aerospace Center (DLR), Institute of Flight Systems, Lilienthalplatz 7, 38108 Braunschweig, Germany

## 1 Introduction

Linear rotorcraft models are essential for flight mechanics analysis, simulation and flight control design, and are often derived from flight test data using system identification techniques. Most of the rotorcraft system identification that is performed uses classical methods such as the frequency domain maximum likelihood (ML) method or the frequency response (FR) method (see Ref. [1]) to derive physics-based linear state-space models of the corresponding vehicle. The identified models can be accurate for frequencies up to 30 rad/s depending on the model complexity, and whether rotor states such as flapping and inflow/coning or engine states such as rotor speed and torque are included. A good overview over high-order rotorcraft modeling for system identification can be found in chapter 15 of Ref. [2].


**Fig. 1** DLR's research helicopter ACT/FHS

But today, state-of-the-art time-domain system identification methods such as the optimized predictor-based subspace identification method (PBSIDopt) also offer the possibility to estimate high-order models from open- and closed-loop data for multiple input and output systems, see Refs. [3, 4]. The PBSIDopt method has been applied to simulated data of the Bo105 helicopter in Ref. [5] and to flight test data of a light utility helicopter prototype in Ref. [6].

The DLR (German Aerospace Center) Institute of Flight Systems operates the ACT/FHS (Active Control Technology/Flying Helicopter Simulator) research helicopter, see Fig. 1. The ACT/FHS is a highly modified Airbus Helicopters (former Eurocopter) EC135, a twin-engine helicopter with a maximum takeoff weight of about 2.9 t, a bearing-less main rotor and a fenestron. The ACT/FHS is equipped with a full-authority fly-by-wire/fly-by-light control system which enhances its mechanical controls. An integrated experimental system is able to apply test control inputs to the ACT/FHS in flight. As the ACT/FHS is not equipped with the standard EC135 stabilization system, its dynamics are not comparable to those of a production EC135 rotorcraft.

Linear models of different complexity for the ACT/FHS have been identified using the classical ML and FR methods (see Refs. [7–11]) leading to physics-based models with a model order of up to $n = 17$. But also the black box PBSIDopt method has been successfully applied to ACT/FHS data. In Ref. [12], a model with an order of $n = 38$ (subsequently reduced to $n = 18$) was identified from flight test data. High-order models including engine effects were identified in Ref. [13], and in Ref. [14] models for handling qualities and dynamic stability prediction were extracted with model orders of $n = 12$ and $n = 18$.

Ideally, a system identification method should work with data from flight tests that are easy to perform and do not need specially trained pilots. The method should provide accuracy information for the identified model parameters as these are necessary for the subsequent use of the models for control system development and simulation. Furthermore, it should be possible to derive models even when no physics-based model structure is available.

As both the classical physics-based and the black box methods have their respective strengths and weaknesses with respect to these requirements, this paper reports on an effort to combine both techniques such that they complement each other.

The paper will first give a short introduction to the applied identification methods. Next, the two techniques will be combined to address the areas of flight test database requirements, parameter accuracy metrics, and model structure specification. Finally, the results will be summarized and more areas, where the two methods might complement each other, will be outlined.

## 2 Applied methods

All of the applied identification methods yield linear state-space models of the form

$$\begin{aligned} \dot{\boldsymbol{x}}(t) &= \boldsymbol{A}\boldsymbol{x}(t) + \boldsymbol{B}\boldsymbol{u}(t) \\ \boldsymbol{y}(t) &= \boldsymbol{C}\boldsymbol{x}(t) + \boldsymbol{D}\boldsymbol{u}(t) \end{aligned} \tag{1}$$

and are based on measured data for the input variables $\boldsymbol{u}$ and output variables $\boldsymbol{y}$.

Regarding the classical methods, the ML method in the time domain minimizes the output errors and the frequency domain ML method optimizes the fit of the output spectra. In contrast, the FR method solves a quadratic cost function to match the frequency responses in amplitude and phase. Optionally, coherence weighting can be used in the FR cost function. This coherence weighting allows an emphasis to be placed on matching the frequency responses in those frequency ranges with the highest coherence and de-weighting data with low coherence.

The PBSIDopt method uses a predictor form model representation in the discrete time domain. The predictor form state-space model allows the system identification problem to be transformed into a high-order vector-ARX model (AutoRegressive model with eXogenous input), which is solved by a linear least-squares problem. Then the estimated ARX parameters are used to reconstruct the model states applying a singular value decomposition. This step can be interpreted as a model reduction step. Next, the discrete-time state-space matrices are estimated in a least-squares sense comprising the inputs, outputs, and the reconstructed system states. Finally, the discrete-time system is transformed into a continuous-time state-space system.

More details about the classical ML and FR methods as well as the PBSIDopt method can be found in Appendix.

The classical identification methods need data from special maneuvers such as frequency sweeps and multistep inputs that have to be performed open loop, thus, requiring specially trained test pilots. In contrast, the PBSIDopt method also works for closed-loop operation and does not require special maneuvers. Of course, sufficient system excitation is needed for all system identification methods. In Ref. [15], generalized binary noise excitation data from closed-loop operation have been shown to give comparable results to open-loop data and simplify system identification flight tests.

For the classical methods, a model structure has to be specified, which is usually derived from physical considerations. Only the model order and two integer parameters (past and future window length) have to be specified for the PBSIDopt method. Then the model states are selected automatically by the algorithm. The resulting models have fully populated system matrices and usually non-physical states. However, the identified model can be transformed in such a way that the first $n_y$ state variables correspond to the output variables using the transformation described in Ref. [13].

The classical identification methods yield Cramer–Rao bounds as accuracy metrics for the identified model parameters. No such metrics are available for the PBSIDopt method.

Table 1 summarizes the characteristics of both identification methods.

## 3 Database

For the classical system identification methods, dedicated flight tests have to be performed to generate a suitable database for identification and validation. Models of the ACT/FHS research helicopter have been identified using these classical frequency domain methods with such flight tests, see Refs. [7, 8, 9–11]. The corresponding database consists of manually flown frequency sweeps and computer-generated multistep maneuvers for all control inputs at various reference speeds. During these open-loop flight test maneuvers, the pilot applied uncorrelated, pulse-type controls to maintain a flight state near the reference trim condition.

Flight test maneuvers for system identification purposes are usually performed open-loop for several reasons. Feedback control suppresses the low-frequency inputs resulting in poor low-frequency identification performance. Furthermore, feedback introduces correlations between multiple inputs and between disturbances and inputs. This results in biased estimates and reduces the off-axis model accuracy for classical frequency domain methods as described in detail in chapters 5.8 and 8 of Ref. [2].

No such strict flight test requirements exist for the PBSIDopt method. The PBSIDopt method operates directly on the measured input–output data and is able to estimate asymptotically unbiased models from noisy closed-loop data, see Refs. [3, 4, 16] or the overview in Ref. [17]. In Refs. [12, 13], models of the ACT/FHS research rotorcraft have been identified by applying the PBSIDopt method to open-loop system identification flight test data. The identified (high-order) models provide very good accuracy and show that the PBSIDopt method is applicable to open-loop rotorcraft system identification flight test data. Furthermore, in Ref. [15], it has been shown that comparable identification results can even be obtained with (generalized) binary noise excitation in closed-loop operation under noisy conditions.

Therefore, the first idea for a complementary use of black box and physics-based identification was as follows:

- use PBSIDopt to identify a high-order black box model from data with binary noise excitation,
- generate frequency response data from this identified model (analytically),
- use this frequency response data to identify a physics-based model with the FR method.

The FR methods needs accurate frequency responses as a basis for the identification of a physics-based model. Usually, the required frequency responses are extracted from flight test data with frequency sweep excitation using segmenting and windowing techniques and applying multi-input/multi-output conditioning and composite windowing techniques as described in chapters 7, 9, and 10 from

**Table 1** Characteristics of the applied identification methods

| ML/FR | PBSIDopt |
|---|---|
| Frequency domain | Time domain |
| Requires special open-loop maneuvers (Frequency sweeps, multistep maneuvers) | Only sufficient excitation required (Works closed-loop and with noise excitation) |
| Model structure including state variables must be specified | Only model order and two integer parameters must be specified |
| Physically meaningful states | State variables selected automatically (non-physical) |
| (Potentially) sparse system matrices | Fully populated system matrices |
| Cramer–Rao bounds as accuracy metrics | No direct parameter accuracy metrics available |

Ref. [2]. Alternatively, the local polynomial method can be used for FR generation, see Ref. [18].

Figure 2 compares the resulting FRs applying the segmenting and windowing technique to data with binary noise and sweep excitation. The data were generated on the ground-based simulator and the sweep inputs were pilot generated. It can be seen that the results differ clearly in the low-frequency region and that the coherence is much lower for the binary noise excitation. Thus, this type of data cannot be used for direct FR extraction.

For the FR generation from the binary noise data with the PBSIDopt method, a model order with $n = 18$ was selected to include the higher order rotor dynamics. The output variables of the PBSIDopt model were chosen as $u$, $v$, $w$, $p$, $q$, $r$, $\phi$, $\theta$, $a_x$, $a_y$, and $a_z$. The linear accelerations were explicitly included as output variables because they are needed by the physics-based model as variables to be matched.

An 8-DoF model with explicit flapping formulation as described in Ref. [19] with a model order of $n = 10$ was then extracted both from FRs generated from sweep data and from the FRs resulting from the PBSIDopt model. As the PBSIDopt model-derived FRs contain no coherence information, the selection of the frequency ranges over which the different FRs shall be matched cannot be based on coherence. For this comparison case, the same frequency ranges as for the sweep-derived FRs were used. Also, no coherence weighting in the cost function could be used for the identification with the PBSIDopt model-derived FRs.

Figure 3 compares the resulting match in pitch rate $q$ and yaw rate $r$ as well as in vertical velocity $w$. (Roll rate $p$ and lateral acceleration $a_y$ are discussed below.) It can be seen that both approaches yield comparable results. The same holds for the eigenvalues of the identified models that are listed in Table 2 and shown in Fig. 4.

This investigation demonstrates that FRs that are derived from a black box model can be used as a database for an identification of a physics-based model. This allows the use of flight test maneuvers for system identification that are not suitable for evaluation with the classical identification methods. A disadvantage is that the frequency responses that are generated from a PBSIDopt model yield no coherence information so that no coherence weighting in the FR method can be used and the selection of the frequency ranges for the different FRs to be matched have to be selected from physical considerations.

Problems with the identification of a physics-based model can arise, when the frequency responses that result from a PBSIDopt model are not physically consistent. For the current investigations, first FRs generated from a 14th-order PBSIDopt model were used. With these FRs, it was not possible to identify a physics-based model that matched the frequency responses for both lateral acceleration and roll rate due to lateral cyclic input at the same time. A sufficient match in $p/\delta_{\mathrm{lat}}$ could only be obtained when de-weighting the match in $a_y/\delta_{\mathrm{lat}}$ and vice versa.

To find a reason for this problem, the FRs for the linear accelerations $a_x, a_y, a_z$ were determined both from the corresponding model output equations and by calculating them from the state equations for the velocity components $\dot{u}, \dot{v}, \dot{w}$ and the output equations for the angular rates $p$, $q$, $r$ and Euler angles $\phi, \theta$ using the trim conditions $(u_0, v_0, w_0, \phi_0, \theta_0)$.

$$
\begin{aligned}
a_x &= \dot{u} + w_0 q - v_0 r + g\cos\theta_0\theta \\
a_y &= \dot{v} + u_0 r - w_0 p - g\cos\phi_0\cos\theta_0\phi + g\sin\phi_0\sin\theta_0\theta \\
a_z &= \dot{w} + v_0 p - u_0 q + g\sin\phi_0\cos\theta_0\phi + g\cos\phi_0\sin\theta_0\theta.
\end{aligned}
\tag{2}
$$

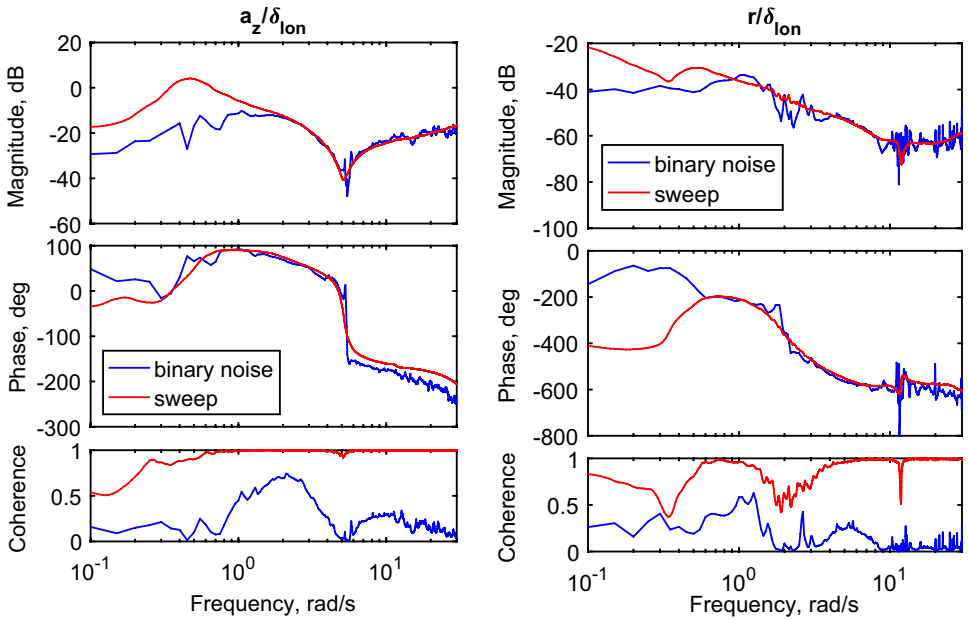


**Fig. 2** Frequency responses generated from binary noise and from sweep excitation

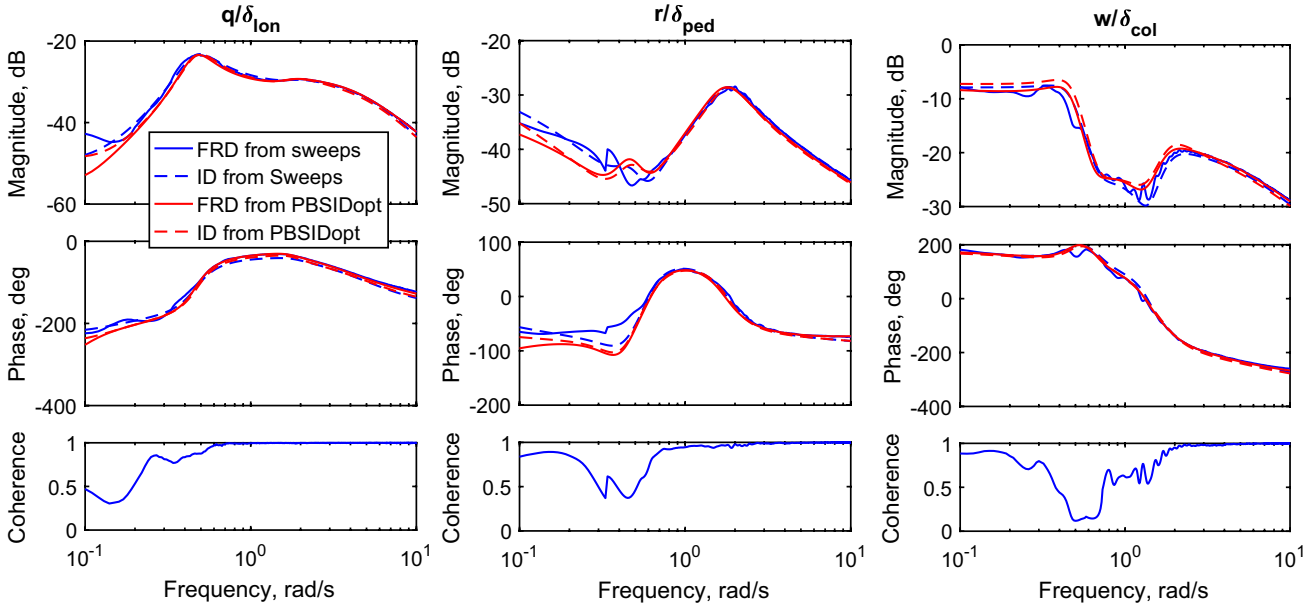


**Fig. 3** Identification using frequency responses from sweeps and from PBSIDopt model (8-DoF, 60 kn)

**Table 2** Eigenvalues of the identified models ($[\zeta, \omega] = s^2 + 2\zeta\omega + \omega^2$), see also Fig. 4

| Mode | Sweep-FR | PBSIDopt-FR |
|---|---|---|
| Spiral | −.0641 | −.0236 |
| Phugoid | [−.266, .465] | [−.233, .476] |
| Pitch | −.472 | −.493 |
| Dutch roll | [.321, 1.81] | [.289, 1.82] |
| Pitch/flap | [.810, 4.96] | [.855, 5.05] |
| Roll/flap | [.760, 10.3] | [.759, 11.3] |

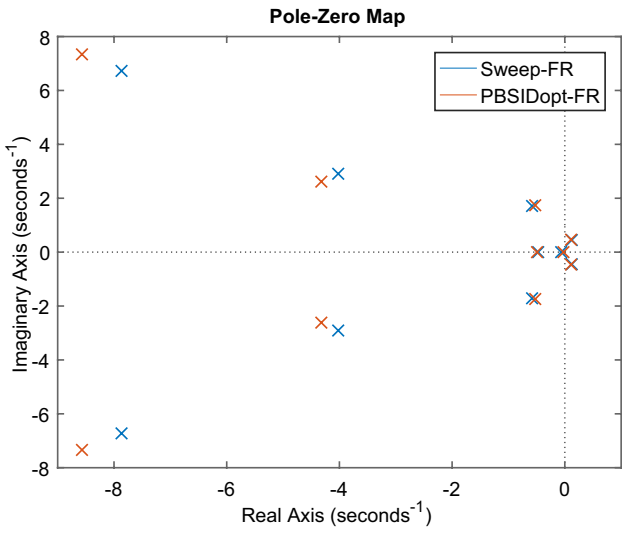


**Fig. 4** Eigenvalues of the identified models shown in Fig. 3 and listed in Table 2 (8-DoF, 60 kn)

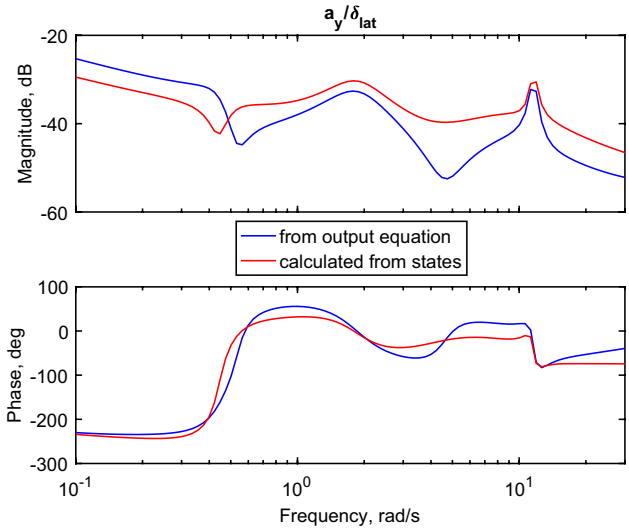


**Fig. 5** $a_y/\delta_{\text{lat}}$ from output equation and calculated from state variables

Figure 5 shows the resulting transfer function for $a_y/\delta_{\text{lat}}$. It can be seen that a clear difference exists, especially in amplitude. Due to the black box approach, the model outputs for the linear velocities $u$, $v$, $w$ and the accelerations $a_x, a_y, a_z$ are not coupled by the kinematic relations, leading to discrepancies when the linearized kinematic equations (2) are applied. This discrepancy is believed to have caused the identification problems.

## 4 Accuracy metrics

The identification process returns the state-space model that best matches the flight test data. A measure of the accuracy or relative degree of confidence of the identification parameters is desirable for several reasons.

- During the identification process of a physics-based model, the information of the relative accuracy of the parameters as well as the information about parameter correlations are used to refine the model. Parameters with low confidence are fixed at physically reasonable values or are eliminated from the model.
- If the identified model is to be used for control system design, a measure of parameter accuracy is needed to analyze and ensure robustness. Many control design procedures use estimates of expected uncertainties in the design process. Once a control system design is completed, the estimated uncertainties are used to evaluate expected degradation with respect to the nominal performance.
- The evaluation of apparent differences between flight test identified and simulation parameters requires knowledge of the level of confidence with which the identified parameters are known.

Reference [20] provides a complete discussion of the mathematical basis for the theoretical accuracy analysis of the classical identification methods. The Cramer–Rao inequality provides the fundamental basis for the theoretical accuracy analysis. The Cramer–Rao bound $\mathrm{CR}_j$ establishes the minimum expected standard deviation.

The Cramer–Rao bound $\mathrm{CR}_j$ of the $j$th identified parameter is determined from the associated diagonal element of the inverse of the Fischer information matrix $\boldsymbol{\mathcal{F}}$

$$\mathrm{CR}_j = \sqrt{(\boldsymbol{\mathcal{F}})^{-1}_{jj}}, \tag{3}$$

where $\boldsymbol{\mathcal{F}}$ is defined as

$$\boldsymbol{\mathcal{F}} = \sum_k \left[\frac{\partial \boldsymbol{y}(k)}{\partial \theta}\right]^{\mathrm{T}} \boldsymbol{R}^{-1} \left[\frac{\partial \boldsymbol{y}(k)}{\partial \theta}\right] \tag{4}$$

and $\boldsymbol{R}$ is the measurement noise covariance matrix. The information matrix is usually determined numerically by evaluating the gradients of the output variables $\boldsymbol{y}$ with respect to perturbations in the converged parameter values.

For subspace identification methods, the analysis of the asymptotic variance has been investigated in Ref. [21] and explicit expressions for it have been derived, but the resulting expressions are very complicated and costly to implement. Therefore, a bootstrap approach was suggested in Ref. [6] to evaluate the standard deviation of invariants of PBSIDopt estimated models, such as the eigenvalues and the transfer functions. This approach, however, does not provide accuracy information for the model parameters (the matrix elements) themselves.

For this reason, the idea for a complementary use of physics-based and black box modeling was as follows:

- Identify a model with the PBSIDopt method.
- Implement the identified model into the ML or FR algorithm and calculate Cramer–Rao bounds for all model parameters (matrix elements).

The test case was an 8th-order model that was identified with the PBSIDopt method from ACT/FHS simulator test data for 60 knots forward flight in a closed-loop experiment design with computer-generated generalized binary noise excitation and a signal-to-noise ratio of 25 (see Ref. [15]).

To make the results easier to compare to derivatives from a classical physics-based model, the PBSIDopt model was first transformed such that the state variables are identical to the output variables using the method described in Ref. [13]. With the chosen output variables of $u$, $v$, $w$, $p$, $q$, $r$, $\phi$, and $\theta$, this corresponds to a classical 6-DoF model.

For comparison, a classical 6-DoF model that was identified with the frequency domain ML output error method from sweep input maneuvers was used. The kinematic coupling terms had to be removed from the state matrix elements of the PBSIDopt model to compare the results for the derivatives of the ML and PBSIDopt models. The corresponding equations are

$$\begin{aligned} X_{\mathrm{q}} &= A(1,5) + w_0, \quad & X_{\mathrm{r}} &= A(1,6) - v_0, \\ Y_{\mathrm{p}} &= A(2,4) - w_0, \quad & Y_{\mathrm{r}} &= A(2,6) + u_0, \\ Z_{\mathrm{p}} &= A(3,4) + v_0, \quad & Z_{\mathrm{q}} &= A(3,5) - u_0, \end{aligned} \tag{5}$$

where $A(i, j)$ denotes the element in the $i$th row and $j$th column of the state matrix $\boldsymbol{A}$.

Figure 6 shows the results obtained for some stability and control derivatives where circles mark the identified values and whiskers the Cramer–Rao uncertainty bounds. It can be seen that both methods yield similar results for the identified derivatives and that the uncertainty bounds of the PBSIDopt model are generally higher than those of the ML-derived model. This is probably partial due to the fact that the PBSIDopt parameter estimates are not ML estimates and thus the statistical properties of the calculated Cramer–Rao bounds do not apply. Furthermore, the system matrices of the PBSIDopt model are fully populated and thus contain more parameters to be estimated.

As the $\boldsymbol{C}$-matrix of the transformed PBSIDopt model is an identity matrix and the $\boldsymbol{D}$-matrix is empty, this results in 64

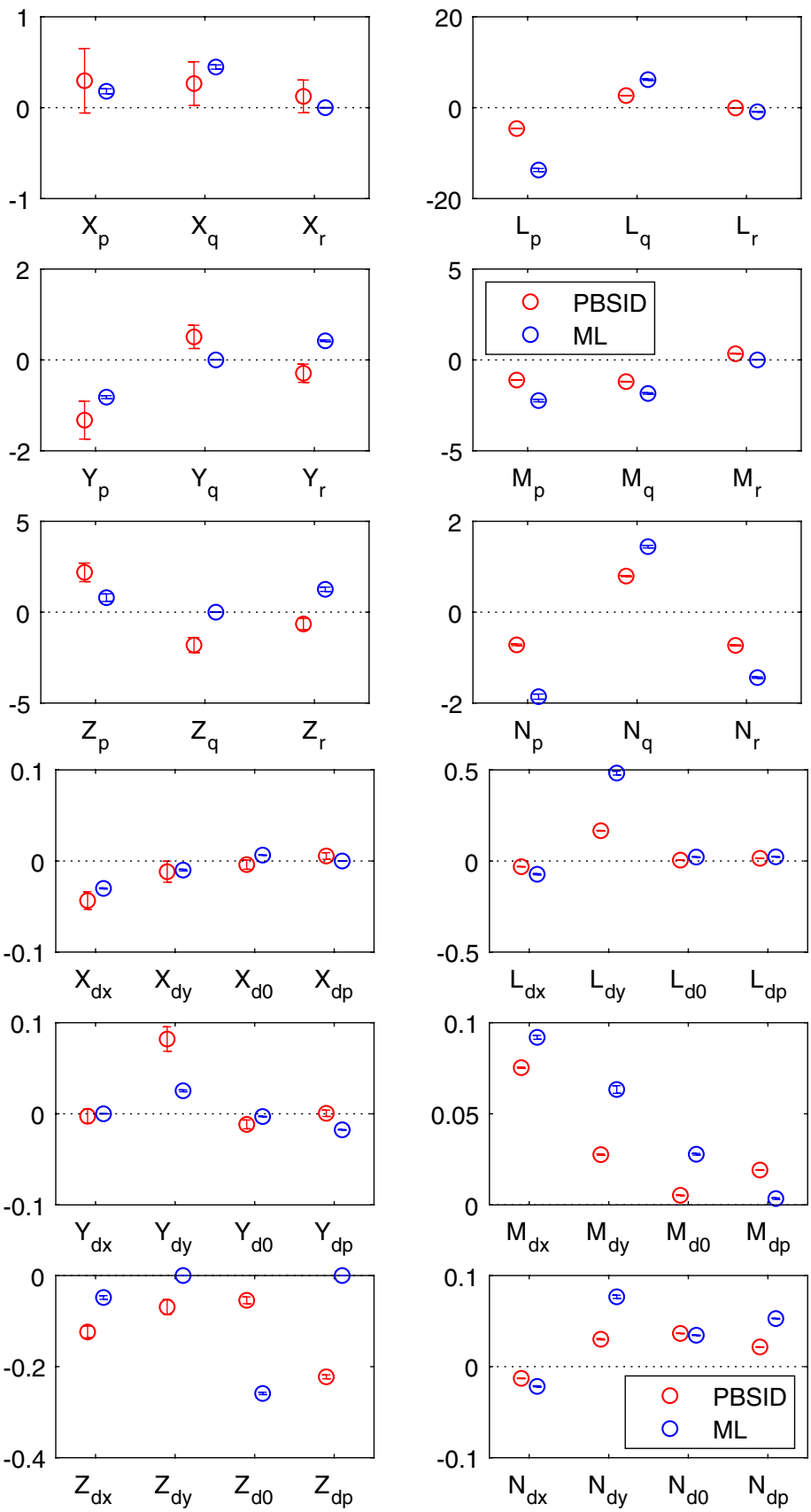


**Fig. 6** Identified stability and control derivatives with corresponding uncertainty bounds

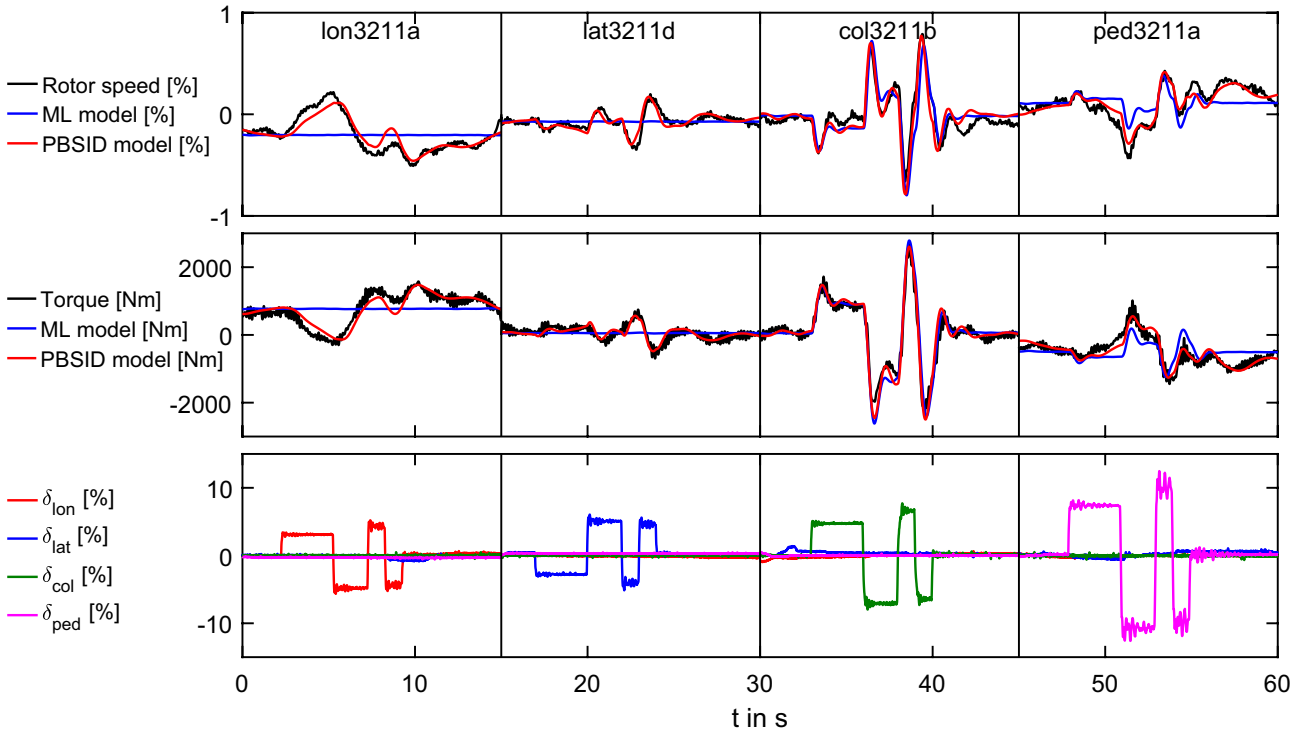


**Fig. 7** Time domain comparison of physics-based (ML) and black box (PBSIDopt) engine model

variable parameters in the $\boldsymbol{A}$-matrix and 32 elements in the $\boldsymbol{B}$-matrix. For the classical 6-DoF model, all matrix elements corresponding to pitch and roll angle are known quantities. This results in a maximum of 36 unknown parameters in the $\boldsymbol{A}$-matrix and a maximum of 24 unknown parameters in the $\boldsymbol{B}$-matrix. Usually, these numbers are further reduced in the model structure determination process. For the present example, the ML-derived model had 46 unknown parameters compared to 96 for the PBSIDopt model.

This example shows that a classical ML or FR identification method can be used to derive CR bounds for the parameters of a PBSIDopt model. However, in the cases investigated by the authors, this approach only worked for model orders of up to $n = 8$. For higher model orders, the large increase in unknown parameters led to numerical problems and excessive correlation between the model parameters, thus preventing the calculation of meaningful accuracy bounds.

## 5 Model structure

Finally, the requirement of specifying a model structure is addressed. Physics-based models are often preferred because of their rather sparse model structure and because they offer physical insight and it is easier to omit certain effects or to split the model into submodels. But sometimes a physics-based model for a subsystem is not available because no measurements of the internal variables exist.

For example, to be able to extract a physics-based engine model from flight test data, it is necessary to have a fuel flow measurement. In ACT/FHS system identification, a model for rotor speed and torque dynamics was needed to account for the torque influence mainly on yaw rate. As no measured engine parameters such as fuel flow or generator speed was available, it was not possible to identify a physics-based engine model.

Therefore, in Ref. [19], a model for rotor speed and torque dynamics was derived from a transfer function approximation and then transformed into a state-space system. This model only covers the response due to collective and pedal inputs and has deficits for pedal inputs in forward flight. The identified model was then coupled with a flight mechanics model including rigid-body and rotor dynamics.

As a physics-based model for the rotor speed and torque dynamics is not necessary in this case, it was tried to identify an improved model with the PBSIDopt method. The inputs for the model were the four pilot controls as well as the vertical velocity $w$ and yaw rate $r$ to account for coupling effects. The outputs were rotor speed and torque, and a model order of $n = 4$ was selected. Figure 7 shows the match for the PBSIDopt model in comparison to the ML-derived

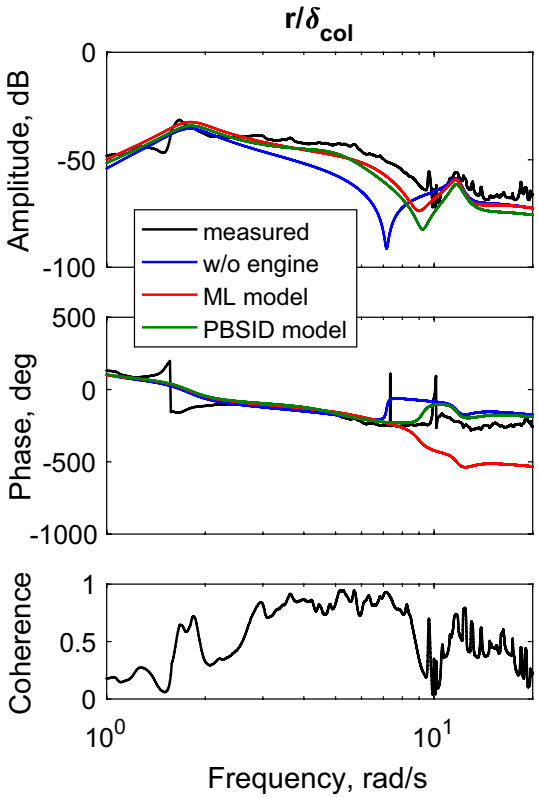


**Fig. 8** Improvement in $r/\delta_{\text{col}}$ by accounting for torque dynamics

model from Ref. [19]. (Rotor speed is given as deviation from trim speed.) It can be seen that both models perform comparably well for collective inputs (third column from the left) but that the PBSIDopt model performs better for all other control inputs. This would be expected because the ML-derived model does not account for the influence of the cyclic control inputs on rotor speed and torque and contains no coupling to $w$ and $r$.

Calculating the Cramer–Rao uncertainty bounds for the PBSIDopt model, as described in the previous section, indicated that more than half of the model parameters could be safely omitted. Thus, a model reduction process was performed with the ML frequency domain method, resulting in a second-order model. This reduced rotor speed/torque model was then coupled to a helicopter model covering the rigid-body and rotor dynamics as described in Ref. [19].

Figure 8 shows that the reduced PBSIDopt engine model performs as well as the transfer function-derived model that was used before regarding the yaw response to collective inputs. Furthermore, the PBSIDopt-derived engine model covers the rotor speed and torque response to other control inputs as well.

This example shows that the PBSIDopt method can be used for (sub)model identification where a physical model structure does not exist and is not required. Performing an accuracy analysis on the resulting model with classical identification methods allows a model reduction to be performed to gain a more robust model.

## 6 Summary and outlook

This paper has shown that black box and physics-based system identification techniques can complement each other and can be combined in the following ways.

1. An identified high-order black box model can be used to generate transfer functions which can then be used as a frequency response database for identifying a physics-based model. This offers the possibility to use flight test data generated in closed-loop operation without specially trained pilots and to reduce flight test time.
2. The FR or ML output error method can be used to get accuracy metrics for the parameters of an identified black box model.
3. Black box modeling can be used for subsystems and these submodels can then be integrated into an overall physics-based model.

Problems that were encountered during the investigations are

1. Transfer functions generated from black box models contain no coherent information; therefore, no coherence weighting can be used in the subsequent identification with the FR method.
2. Transfer functions that are generated from a black box model might be physically inconsistent. This can cause problems in fitting a physics-based model to these data.
3. Extracting accuracy metrics for parameters from a fully populated black box model was successfully performed for model orders of up to $n = 8$. For higher model orders, numerical problems and excessive correlation prevented the calculation of meaningful accuracy bounds.

For the future, it is planned to use black box identification also for modeling the remaining deficits of a physics-based model. In Ref. [22], these model deficits are described as parametric input filters (pilot remnants) to be added to the system inputs. The calculated pilot remnants are derived using inverse simulation techniques and are then approximated by low-order transfer function models. Alternatively, a linear black box MIMO system could be used for this purpose.

## Appendix: Applied identification methods

### Symbols

| | |
|---|---|
| $\boldsymbol{A}_d, \boldsymbol{B}_d, \boldsymbol{C}_d, \boldsymbol{D}_d$ | Discrete-time state-space matrices |
| $\boldsymbol{A}_K, \boldsymbol{B}_K$ | Predictor form state-space matrices |
| $\boldsymbol{e}_k, \boldsymbol{u}_k, \boldsymbol{x}_k, \boldsymbol{y}_k$ | Discrete-time innovation, input, state, and output vectors at $k$th time step |
| $\boldsymbol{E}, \boldsymbol{U}, \boldsymbol{X}, \boldsymbol{Y}$ | Data matrices for system innovation, input, state, and output |
| $f, p$ | Future and past window length |
| $\boldsymbol{K}$ | Kalman gain matrix |
| $\mathcal{K}^{(p)}$ | Extended controllability matrix |
| $M_f, M_n, M_p$ | Sets for $f$, $n$ and $p$ |
| $n_u$ | Number of model inputs |
| $N$ | Number of data points |
| $\mathcal{O}^{(f)}$ | Extended observability matrix |
| $s$ | Laplace variable (1/s) |
| $\boldsymbol{\mathcal{S}}$ | Diagonal singular values matrix |
| $\boldsymbol{T}$ | Frequency response matrix |
| $w_{\mathrm{ap}}$ | Relative weighting amplitude/phase errors |
| $w_\gamma$ | Coherence weighting |
| $\boldsymbol{y}_{\mathrm{m},k}$ | Measured output (index m) |
| $\boldsymbol{z}_k$ | Merged input–output vector at $k$th time step |
| $\boldsymbol{Z}$ | Data matrices for merged input–outputs (used with indexes) |
| $\gamma^2_{uy}$ | Coherence between $u$ and $y$ |
| $\lambda$ | Regularization parameter |
| $\omega$ | Angular frequency (rad/s) |
| $\sigma(\ldots)$ | Standard deviation |
| $\tau$ | Time delay (s) |
| $\measuredangle$ | Phase angle (°) |
| $\lvert \ldots \rvert_{\mathrm{dB}}$ | Amplitude (dB) |

### ML output error method

The system to be identified is assumed to be described by a linear state-space model

$$\begin{aligned}\dot{\boldsymbol{x}}(t) &= \boldsymbol{A}(\boldsymbol{\Theta})\boldsymbol{x}(t) + \boldsymbol{B}(\boldsymbol{\Theta})\boldsymbol{u}(t)\\ \boldsymbol{y}(t) &= \boldsymbol{C}(\boldsymbol{\Theta})\boldsymbol{x}(t) + \boldsymbol{D}(\boldsymbol{\Theta})\boldsymbol{u}(t),\end{aligned} \tag{6}$$

where $\boldsymbol{x}$ denotes the state vector, $\boldsymbol{u}$ the input vector and $\boldsymbol{y}$ the output vector. The system matrices $\boldsymbol{A}$, $\boldsymbol{B}$, $\boldsymbol{C}$ and $\boldsymbol{D}$ contain the unknown model parameters $\boldsymbol{\Theta}$. Measurements $\boldsymbol{z}$ of the outputs exist for $N$ discrete time points $t_k$

$$\boldsymbol{z}_k = \boldsymbol{y}(t_k) + \boldsymbol{v}(t_k)\,, \quad k = 1, \ldots, N. \tag{7}$$

The measurement noise $\boldsymbol{v}$ is assumed to be characterized by Gaussian white noise with covariance matrix $\boldsymbol{R}$.

The ML estimates of the unknown parameters $\boldsymbol{\Theta}$ and of the measurement noise covariance matrix $\boldsymbol{R}$ are obtained by minimizing the cost function

$$\begin{aligned}J(\boldsymbol{\Theta}, \boldsymbol{R}) = \frac{1}{2}\sum_{k=1}^{N} &\left[\boldsymbol{z}(t_k) - \boldsymbol{y}(t_k)\right]^T \boldsymbol{R}^{-1}\\ &\times \left[\boldsymbol{z}(t_k) - \boldsymbol{y}(t_k)\right] + \frac{N}{2}\ln\left(\det\left(\boldsymbol{R}\right)\right).\end{aligned} \tag{8}$$

If the measurement error covariance matrix $\boldsymbol{R}$ is unknown, as it is usually the case, the optimization of Eq. (8) is carried out in two steps. In the first step, it can be shown that for any given value of $\boldsymbol{\Theta}$, the ML estimate of $\boldsymbol{R}$ is given by

$$\boldsymbol{R} = \frac{1}{N}\sum_{k=1}^{N}\left[\boldsymbol{z}(t_k) - \boldsymbol{y}(t_k)\right]\left[\boldsymbol{z}(t_k) - \boldsymbol{y}(t_k)\right]^T \tag{9}$$

which means that the output error covariance matrix is the most plausible estimate for $\boldsymbol{R}$.

Thus, the variable part of the cost function reduces to

$$J(\boldsymbol{\Theta}) = \ln\left(\det\left(\boldsymbol{R}\right)\right). \tag{10}$$

If the covariance matrix $\boldsymbol{R}$ is assumed to be a diagonal matrix, the cost function reduces to the product of the output error variances of all output variables

$$J(\boldsymbol{\Theta}) = \prod_{j=1}^{n_y}\left(\frac{1}{N}\sum_{k=1}^{N}\left[z_j(t_k) - \boldsymbol{y}_j(t_k)\right]^2\right). \tag{11}$$

*Frequency domain variant*

The discretely sampled time-dependent variable

$$\boldsymbol{x}_k = \boldsymbol{x}(k\Delta t)\,, \quad k = 0, \ldots, N-1 \tag{12}$$

with the sampling time interval $\Delta t$ is transformed to a frequency-dependent variable using the Fourier transform

$$\begin{aligned}\boldsymbol{x}(\omega_k) &= \frac{1}{N}\sum_{k=0}^{N-1}\boldsymbol{x}_k \mathrm{e}^{-\mathrm{i}\omega_k k\Delta t}\\ \omega_k &= k\cdot 2\pi/t_N \;\text{ with }\; t_N = (N-1)\Delta t\,.\end{aligned} \tag{13}$$

Transforming the variables $\dot{\boldsymbol{x}}$, $\boldsymbol{x}$, $\boldsymbol{u}$, $\boldsymbol{y}$ of the linear model from Eq. (6) to the frequency domain leads to the following model equations in the frequency domain

$$\begin{aligned}\mathrm{i}\omega\boldsymbol{x}(\omega) &= \boldsymbol{A}(\boldsymbol{\Theta})\boldsymbol{x}(\omega) + \boldsymbol{B}(\boldsymbol{\Theta})\boldsymbol{u}(\omega)\\ \boldsymbol{y}(\omega) &= \boldsymbol{C}(\boldsymbol{\Theta})\boldsymbol{x}(\omega) + \boldsymbol{D}(\boldsymbol{\Theta})\boldsymbol{u}(\omega).\end{aligned} \tag{14}$$

The ML cost function in the frequency domain is derived analogously to the one in the time domain with the output error covariance matrix $\boldsymbol{R}$ replaced by the spectral density

matrix of the measurement noise. The ML cost function in the frequency domain is, therefore,

$$J(\boldsymbol{\Theta}) = \prod_{i=j}^{n_y} \boldsymbol{\sigma}^2\left(\boldsymbol{z}_j - \boldsymbol{y}_j\right) \tag{15}$$

with

$$\boldsymbol{\sigma}^2\left(\boldsymbol{z}_j - \boldsymbol{y}_j\right) = \frac{1}{N}\sum_{k=0}^{N-1}\left[\boldsymbol{z}_j(\omega_k) - \boldsymbol{y}_j(\omega_k)\right]^*\left[\boldsymbol{z}_j(\omega_k) - \boldsymbol{y}_j(\omega_k)\right], \tag{16}$$

where $(.)^*$ denotes the conjugate transpose of a complex value and $\boldsymbol{\sigma}^2(.)$ the model error variance.

Minimization of the cost function from Eq. (11) or Eq. (15) is performed using, e.g., a Gauss–Newton optimization method.

## Frequency response method

The ML method in the frequency domain is based on matching the Fourier transform of the output variables. In contrast, the frequency response method is based on matching the frequency responses, i.e., the ratio of the output per unit of control input as a function of control input frequency.

The frequency response matrix of the identification model $\boldsymbol{T}(s)$ relates the Laplace transform $\boldsymbol{Y}(s)$ of the output vector $\boldsymbol{y}$ to the Laplace transform $\boldsymbol{U}(s)$ of the input vector $\boldsymbol{u}$:

$$\boldsymbol{Y}(s) = \boldsymbol{T}(s)\boldsymbol{U}(s). \tag{17}$$

For the linear state-space system from Eq. (6), the frequency response matrix is determined as

$$\boldsymbol{T}(s) = \boldsymbol{C}(s\boldsymbol{I} - \boldsymbol{A})^{-1}\boldsymbol{B} + \boldsymbol{D}, \tag{18}$$

where $\boldsymbol{I}$ denotes the identity matrix.

The quadratic cost function to be minimized for the frequency response method is

$$J = \frac{20}{N_\omega}\sum_{k=1}^{N\omega} w_\gamma(k)\Big[\left(|T_\mathrm{m}(k)|_{dB} - |T(k)|_{dB}\right)^2 + w_{ap}\left(\measuredangle T_\mathrm{m}(k) - \measuredangle T(k)\right)^2\Big], \tag{19}$$

where $T$ and $T_\mathrm{m}$ are a single-frequency response and its measured counterpart. $N_\omega$ is the number of frequency points in the frequency interval $[\omega_1, \omega_{N\omega}]$. $|\ldots|_{dB}$ denotes the amplitude in dB and $\measuredangle(\ldots)$ the phase angle in degree.

$w_\gamma$ is an optional weighting function based on the coherence between the input and the output at each frequency. It is defined as

$$w_\gamma(k) = \left[1.58(1 - e^{\gamma_{xy}^2(k)})\right]^2, \tag{20}$$

$w_\mathrm{ap}$ is the relative weight between amplitude and phase errors. The normal convention is $w_\mathrm{ap} = 0.01745$.

When several frequency responses are approximated together, the overall cost function is the average of the individual cost functions. A good overview of system identification using the frequency response method can be found in Ref. [2].

## PBSIDopt method

The starting point for the PBSIDopt method is a linear discrete-time state-space model in innovation form

$$\begin{aligned}\boldsymbol{x}_{k+1} &= \boldsymbol{A}_d\boldsymbol{x}_k + \boldsymbol{B}_d\boldsymbol{u}_k + \boldsymbol{K}\boldsymbol{e}_k\\ \boldsymbol{y}_k &= \boldsymbol{C}_d\boldsymbol{x}_k + \boldsymbol{D}_d\boldsymbol{u}_k + \boldsymbol{e}_k\end{aligned} \tag{21}$$

with the input vector $\boldsymbol{u}_k \in \mathbb{R}^{n_u}$, the outputs $\boldsymbol{y}_k \in \mathbb{R}^{n_y}$ and the states $\boldsymbol{x}_k \in \mathbb{R}^n$. The innovations $\boldsymbol{e}_k \in \mathbb{R}^{n_y}$ are assumed to be zero-mean white process noise. A finite set of data points $\boldsymbol{u}_k$ and $\boldsymbol{y}_k$ with $k = 1 \ \ldots N$ is considered for system identification.

Assuming there is no direct feedthrough, i.e., $\boldsymbol{D}_\mathrm{d} = \boldsymbol{0}$, the system in Eq. (21) is transformed to the one-step-ahead predictor form

$$\begin{aligned}\boldsymbol{x}_{k+1} &= \boldsymbol{A}_K\boldsymbol{x}_k + \boldsymbol{B}_K\boldsymbol{z}_k\\ \boldsymbol{y}_k &= \boldsymbol{C}_\mathrm{d}\boldsymbol{x}_k + \boldsymbol{e}_k\end{aligned} \tag{22}$$

with $\boldsymbol{A}_K = \boldsymbol{A}_\mathrm{d} - \boldsymbol{K}\boldsymbol{C}_\mathrm{d}$, $\boldsymbol{B}_K = \begin{pmatrix}\boldsymbol{B}_\mathrm{d} & \boldsymbol{K}\end{pmatrix}$ and $\boldsymbol{z}_k = (\boldsymbol{u}_k \ \ \boldsymbol{y}_k)^T$. Furthermore, it is assumed that all eigenvalues of $\boldsymbol{A}_K$ are inside the unit circle. Accordingly, the given predictor model is stable. The $(k+p)$th state $\boldsymbol{x}_{k+p}$ is given by

$$\begin{aligned}\boldsymbol{x}_{k+p} &= \boldsymbol{A}_K\boldsymbol{x}_{k+p-1} + \boldsymbol{B}_K\boldsymbol{z}_{k+p-1}\\ &= \boldsymbol{A}_K^p\boldsymbol{x}_k + \underbrace{\begin{pmatrix}\boldsymbol{A}_K^{p-1}\boldsymbol{B}_K & \boldsymbol{A}_K^{p-2}\boldsymbol{B}_K & \ldots & \boldsymbol{B}_K\end{pmatrix}}_{\mathcal{K}^{(p)}}\begin{pmatrix}\boldsymbol{z}_k\\ \boldsymbol{z}_{k+1}\\ \vdots\\ \boldsymbol{z}_{k+p-1}\end{pmatrix}\end{aligned} \tag{23}$$

and the $(k+p)$th output $\boldsymbol{y}_{k+p}$ is determined

$$\boldsymbol{y}_{k+p} = \boldsymbol{C}_\mathrm{d}\boldsymbol{A}_K^p\boldsymbol{x}_k + \boldsymbol{C}_\mathrm{d}\mathcal{K}^{(p)}\begin{pmatrix}\boldsymbol{z}_k\\ \boldsymbol{z}_{k+1}\\ \vdots\\ \boldsymbol{z}_{k+p-1}\end{pmatrix} + \boldsymbol{e}_{k+p} \tag{24}$$

with the extended controllability matrix $\mathcal{K}^{(p)}$ and the past window length $p$. Since $\boldsymbol{A}_K$ is stable, the expression $\boldsymbol{A}_K^p$ in Eqs. (23) and (24) can be neglected for large $p$: $\boldsymbol{A}_K^p \simeq \boldsymbol{0}$. Therefore, repeating Eqs. (23) and (24) for the $(p+1)$th in the $N$th element yields

$$\boldsymbol{X}_{(p+1,N)} = \mathcal{K}^{(p)}\boldsymbol{Z}_{(1,N-p),p} \tag{25a}$$

$$\boldsymbol{Y}_{(p+1,N)} = \boldsymbol{C}_\mathrm{d}\boldsymbol{\mathcal{K}}^{(p)}\boldsymbol{Z}_{(1,N-p),p} + \boldsymbol{E}_{(p+1,N)} \tag{25b}$$

with

$$\boldsymbol{X}_{(p+1,N)} = \begin{pmatrix} \boldsymbol{x}_{p+1} & \boldsymbol{x}_{p+2} & \dots & \boldsymbol{x}_N \end{pmatrix} \tag{26}$$

and analogous definitions for $\boldsymbol{Y}_{(p+1,N)}$ and $\boldsymbol{E}_{(p+1,N)}$. The merged inputs and outputs are combined as

$$\boldsymbol{Z}_{(1,N-p),p} = \begin{pmatrix} z_1 & z_2 & \dots & z_{N-p} \\ z_2 & z_3 & \dots & z_{N-p+1} \\ \vdots & \vdots & \dots & \vdots \\ z_p & z_{p+1} & \dots & z_{N-1} \end{pmatrix}. \tag{27}$$

The predictor Markov parameters $\boldsymbol{C}_\mathrm{d}\boldsymbol{\mathcal{K}}^{(p)}$ are estimated in a least-squares sense with Tikhonov regularization to prevent ill-posed problems. The regularized least-squares problem is given by

$$\min_{\boldsymbol{C}_\mathrm{d}\boldsymbol{\mathcal{K}}^{(p)}} \left( \left\| \boldsymbol{Y}_{(p+1,N)} - \boldsymbol{C}_\mathrm{d}\boldsymbol{\mathcal{K}}^{(p)}\boldsymbol{Z}_{(1,N-p),p} \right\|_F^2 + \lambda^2 \left\| \boldsymbol{C}_\mathrm{d}\boldsymbol{\mathcal{K}}^{(p)} \right\|_F^2 \right). \tag{28}$$

The regularization parameter $\lambda$ is chosen with the strong robust generalized cross-validation method, see Ref. [23] for an introduction and a comparison of parameter choice methods.

The estimated predictor Markov parameters $\boldsymbol{C}_\mathrm{d}\boldsymbol{\mathcal{K}}^{(p)}$ can be interpreted as a high-order vector-ARX model (AutoRegressive model with eXogenous input). High-order ARX models based on Eq. (25b) are asymptotically unbiased by correlation issues for large $N$ and $p$, see Ref. [24]. Thus, this step is essential for subspace identification methods such as PBSIDopt to provide consistent estimates even in correlated closed-loop experiments.

Defining the extended observability matrix $\boldsymbol{\mathcal{O}}^{(f)}$ with the future window length $f$

$$\boldsymbol{\mathcal{O}}^{(f)} = \begin{pmatrix} \boldsymbol{C}_\mathrm{d} \\ \boldsymbol{C}_\mathrm{d}\boldsymbol{A}_K \\ \vdots \\ \boldsymbol{C}_\mathrm{d}\boldsymbol{A}_K^{f-1} \end{pmatrix}, \tag{29}$$

the product of the extended observability matrix $\boldsymbol{\mathcal{O}}^{(f)}$ and the extended controllability matrix $\boldsymbol{\mathcal{K}}^{(p)}$ is set up using the estimated predictor Markov parameters $\boldsymbol{C}_\mathrm{d}\boldsymbol{\mathcal{K}}^{(p)}$

$$\boldsymbol{\mathcal{O}}^{(f)}\boldsymbol{\mathcal{K}}^{(p)} \simeq \begin{pmatrix} \boldsymbol{C}_\mathrm{d}\boldsymbol{A}_K^{p-1}\boldsymbol{B}_K & \boldsymbol{C}_\mathrm{d}\boldsymbol{A}_K^{p-2}\boldsymbol{B}_K & \dots & \boldsymbol{C}_\mathrm{d}\boldsymbol{B}_K \\ \boldsymbol{0} & \boldsymbol{C}_\mathrm{d}\boldsymbol{A}_K^{p-1}\boldsymbol{B}_K & \dots & \boldsymbol{C}_\mathrm{d}\boldsymbol{A}_K\boldsymbol{B}_K \\ \vdots & \ddots & \ddots & \vdots \\ \boldsymbol{0} & & & \boldsymbol{C}_\mathrm{d}\boldsymbol{A}_K^{f-1}\boldsymbol{B}_K. \end{pmatrix} \tag{30}$$

According to Eq. (25a)

$$\begin{aligned} \boldsymbol{\mathcal{O}}^{(f)}\boldsymbol{X}_{(p+1,N)} &= \boldsymbol{\mathcal{O}}^{(f)}\boldsymbol{\mathcal{K}}^{(p)}\boldsymbol{Z}_{(1,N-p),p} \\ &= \boldsymbol{\mathcal{U}}\boldsymbol{\mathcal{S}}\boldsymbol{\mathcal{V}}^T \\ &= \begin{pmatrix} \boldsymbol{\mathcal{U}}_n & \boldsymbol{\mathcal{U}}_{\bar{n}} \end{pmatrix} \begin{pmatrix} \boldsymbol{\mathcal{S}}_n & \boldsymbol{0} \\ \boldsymbol{0} & \boldsymbol{\mathcal{S}}_{\bar{n}} \end{pmatrix} \begin{pmatrix} \boldsymbol{\mathcal{V}}_n^T \\ \boldsymbol{\mathcal{V}}_{\bar{n}}^T \end{pmatrix}, \end{aligned} \tag{31}$$

the singular value decomposition is applied to reconstruct an estimation of the system states

$$\widetilde{\boldsymbol{X}}_{(p+1,N)} = \boldsymbol{\mathcal{S}}_n^{\frac{1}{2}}\boldsymbol{\mathcal{V}}_n^T. \tag{32}$$

The model order $n$ corresponds to the $n$ largest singular values in $\boldsymbol{\mathcal{S}}_n$ used for the state sequence reconstruction.

Finally, the system matrices $\boldsymbol{A}_\mathrm{d}$, $\boldsymbol{B}_\mathrm{d}$, $\boldsymbol{C}_\mathrm{d}$ and $\boldsymbol{K}$ from Eq. (21) are calculated. First,

$$\begin{pmatrix} \widetilde{\boldsymbol{X}}_{(\mathrm{p}+2,N)} \\ \boldsymbol{Y}_{(\mathrm{p}+1,N-1)} \end{pmatrix} = \begin{pmatrix} \boldsymbol{A}_\mathrm{d} & \boldsymbol{B}_\mathrm{d} \\ \boldsymbol{C}_\mathrm{d} & \boldsymbol{0} \end{pmatrix} \begin{pmatrix} \widetilde{\boldsymbol{X}}_{(\mathrm{p}+1,N-1)} \\ \boldsymbol{U}_{(\mathrm{p}+1,N-1)} \end{pmatrix} \tag{33}$$

is solved for $\boldsymbol{A}_\mathrm{d}$, $\boldsymbol{B}_\mathrm{d}$ and $\boldsymbol{C}_\mathrm{d}$ in a least-squares sense. The Kalman gain $\boldsymbol{K}$ is then calculated from the covariance matrix of the least-squares residuals and the system matrices $\boldsymbol{A}_\mathrm{d}$ and $\boldsymbol{C}_\mathrm{d}$ by solving the stabilizing solution of the corresponding discrete-time algebraic Riccati equation, see Ref. [24] and the references therein.

The inverse bilinear (or any other discrete time to continuous time) transform is then applied to calculate the continuous-time state-space model:

$$\begin{aligned} \dot{\boldsymbol{x}}(t) &= \boldsymbol{A}\boldsymbol{x}(t) + \boldsymbol{B}\boldsymbol{u}(t) \\ \boldsymbol{y}(t) &= \boldsymbol{C}\boldsymbol{x}(t). \end{aligned} \tag{34}$$

Selecting only the largest $n$ singular values to reconstruct the state sequence in Eq. (32) already corresponds to a model reduction step. If necessary, further model reduction techniques as described in Ref. [12] can be used to adapt a high-order black box model to the frequency range of interest or to reduce its complexity. In the examples presented in this paper, no further model reduction techniques were applied.

## References


1. Hamel, P., Jategaonkar, R.: Evolution of flight vehicle system identification. J. Aircraft **33**(1), 9–28 (1996)
2. Tischler, M.B., Remple, R.K.: Aircraft and Rotorcraft System Identification: Engineering Methods with Flight-Test Examples, 2nd edn. American Institute of Aeronautics and Astronautics Inc, Reston (2012)
3. Chiuso, A.: The role of vector autoregressive modeling in predictor-based subspace identification. Automatica **43**(6), 1034–1048 (2007). https://doi.org/10.1016/j.automatica.2006.12.009

4. Chiuso, A.: On the asymptotic properties of closed-loop CCA-type subspace algorithms: equivalence results and role of the future horizon. IEEE Trans. Autom. Control **55**(3), 634–649 (2010). https://doi.org/10.1109/TAC.2009.2039239
5. Bergamasco, M., Lovera, M.: Continuous-time predictor-based subspace identification for helicopter dynamics. In: 37th European Rotorcraft Forum. Gallarate, Italy (2011)
6. Bergamasco, M., Cortigiani, N., Del Gobbo, D., Panza, S., Lovera, M.: The role of black-box models in rotorcraft attitude control. In: 43rd European Rotorcraft Forum. Milano, Italy (2017)
7. Greiser, S., Seher-Weiss, S.: A contribution to the development of a full flight envelope quasi-nonlinear helicopter simulation. CEAS Aeronaut. J. **5**(1), 53–66 (2014). https://doi.org/10.1007/s13272-013-0090-z
8. Seher-Weiss, S.: Comparing different approaches for modeling the vertical motion of the EC 135. CEAS Aeronaut. J. **6**(3), 395–406 (2015). https://doi.org/10.1007/s13272-015-0150-7
9. Seher-Weiss, S., von Gruenhagen, W.: Development of EC 135 turbulence models via system identification. Aerosp. Sci. Technol. **23**(1), 43–52 (2012). https://doi.org/10.1016/j.ast.2011.09.008
10. Seher-Weiss, S., von Grünhagen, W.: EC 135 system identification for model following control and turbulence modeling. In: 1st CEAS European Air and Space Conference, pp. 2439–2447. Berlin, Germany (2007)
11. Seher-Weiss, S., von Grünhagen, W.: Comparing explicit and implicit modeling of rotor flapping dynamics for the EC 135. CEAS Aeronaut. J. **5**(3), 319–332 (2014). https://doi.org/10.1007/s13272-014-0109-0
12. Wartmann, J., Seher-Weiss, S.: Application of the predictor-based subspace identification method to rotorcraft system identification. In: 39th European Rotorcraft Forum. Moscow, Russia (2013)
13. Wartmann, J.: ACT/FHS system identification including engine torque and main rotor speed using the PBSIDopt method. In: 41st European Rotorcraft Forum. Munich, Germany (2015)
14. Wartmann, J., Greiser, S.: Identification and selection of rotorcraft candidate models to predict handling qualities and dynamic stability. In: 44th European Rotorcraft Forum. Delft, The Netherlands (2018)
15. Wartmann, J.: Closed-loop rotorcraft system identification using generalized binary noise. In: AHS 73rd Annual Forum. Fort Worth, TX (2017)
16. Chiuso, A.: On the relation between CCA and predictor-based subspace identification. IEEE Trans. Autom. Control **52**(10), 1795–1812 (2007). https://doi.org/10.1109/TAC.2007.906159
17. van der Veen, G., van Wingerden, J.W., Bergamasco, M., Lovera, M., Verhaegen, M.: Closed-loop subspace identification methods: an overview. IET Control Theory Appl. **7**(10), 1339–1358 (2013). https://doi.org/10.1049/iet-cta.2012.0653
18. Fragniére, B., Wartmann, J.: Local polynomial method frequency-response calculation for rotorcraft applications. In: AHS 71st Annual Forum. Virginia Beach, VA (2015)
19. Seher-Weiß, S.: ACT/FHS system identification including rotor and engine dynamics. In: AHS 73rd Annual Forum. Fort Worth, TX (2017)
20. Maine, R.E., Iliff, K.W.: Theory and practice of estimating the accuracy of dynamic flight-determined coefficients. Tech. Rep. RP 1077, NASA (1981)
21. van Wingerden, J.W.: The asymptotic variance of the PBSIDopt algorithm. IFAC Proc. Vol. **45**(16), 1167–1172 (2012). https://doi.org/10.3182/20120711-3-BE-2027.00228
22. Greiser, S., von Gruenhagen, W.: Improving system identification results combining a physics-based stitched model with transfer function models obtained through inverse simulation. In: American Helicopter Society 72nd Annual Forum. West Palm Beach, Florida, USA (2016)
23. Bauer, F., Lukas, M.A.: Comparing parameter choice methods for regularization of ill-posed problems. Math. Comput. Simul. **81**(9), 1795–1841 (2011)
24. Ljung, L., McKelvey, T.: Subspace identification from closed loop data. Signal Process. **52**(2), 209–215 (1996). https://doi.org/10.1016/0165-1684(96)00054-0